

Article

# A Multi-Scale Modeling of CH<sub>4</sub> and H<sub>2</sub>O Adsorption on Coal Molecules and the Water Blocking Effect in Coalbed Methane Extraction

Yanhui Yang<sup>1</sup>, Ling Lin<sup>2</sup>, Mengxi Li<sup>1</sup>, Xueying Zhang<sup>1</sup>, Chunli Yang<sup>1</sup>, Yuting Wang<sup>1</sup>, Bin Fan<sup>1</sup>, Congmei Chen<sup>3</sup> and Wenjia Luo<sup>2,\*</sup> 

<sup>1</sup> PetroChina Huabei Oilfield Company, No. 1 Jianshe Middle Road, Renqiu City, Hebei 062552, China

<sup>2</sup> School of Chemistry and Chemical Engineering, Southwest Petroleum University, Chengdu 610500, China

<sup>3</sup> National Supercomputing Center in Shenzhen, Shenzhen 518055, China

\* Correspondence: luowenjia@swpu.edu.cn

Received: 24 July 2019; Accepted: 13 August 2019; Published: 19 August 2019



**Abstract:** Coalbed methane (CBM) is of great economic value. However, at the same time, CBM is facing a multitude of technological challenges. The water blocking effect (WBE) is one of the physical effects that controls the production of CBM. To alleviate WBE, it is necessary to study its mechanisms at the molecular level. In this study, we used a combined first-principles calculation and molecular simulation approach to investigate the adsorption and diffusion of both methane and water in coal. The results suggest that water does not compete with methane in the adsorption on coal surfaces, yet the presence of water significantly slows down the diffusion of methane within the micropores of coal. This work not only explains the fundamental mechanisms of the WBE but also provides a simulation framework for building strategies to alleviate WBE.

**Keywords:** coalbed methane (CBM); density functional theory (DFT); adsorption; molecular dynamics; water blocking effect (WBE)

## 1. Introduction

Coalbed methane (CBM) is one kind of natural gas found in a coal reservoir [1]. A report by Mastalerz et al. shows that, in 2014, the global CBM production reached over 240 billion cubic meters [2]. Despite its large production and considerable economic value, CBM is fundamentally different from the conventional gas, and its production put forward numerous scientific and technical challenges [3,4]. It is generally presumed that gas holding capacity and permeability are two important factors which characterize a CBM reservoir. The former factor determines the gas capacity of the reservoir, while the latter one suggests the easiness of gas extraction [1]. Moreover, CBM is often found with other components, including water and carbon dioxide, in the coal reservoir. Water can also be introduced into the coalbed via hydraulic fracturing during well development processes. Therefore, a study on the adsorption and diffusion behaviors of methane on coal, especially in the presence of water, can generate a better understanding of CBM reservoirs and provide insights on the development of the exploration technologies.

Methane adsorption in the coal matrix has been widely studied at the molecular level by using both first-principles methods [5–10] and molecular simulation techniques [11–16]. These works provide valuable insights into the mechanisms of methane adsorption and diffusion in the coal matrix. However, there are still several topics which are not fully discussed, as follows: 1. The molecular models for coal used in previous first-principles studies are often simplified as graphene or a single carbon sheet, while the effect of other functional groups in coal is neglected. 2. The effect of water, including its

competitive adsorption with methane and its effect on methane diffusion, is not fully covered. However, in engineering practice, it has been found that the water blocking effect (WBE) is one of the major reasons that limit the production rate of CBM wells [17–20]. 3. The effect of microstructures, including micropores, are usually not considered in previous molecular models, although it is generally believed that methane is held within micropores in the CBM reservoirs.

In this study, we aim at bridging these gaps above by performing a combined density-functional theory (DFT) and molecular dynamics (MD) study, with emphasis on the effect of functional groups in coal, the competitive adsorption between water and methane, and the desorption and diffusion of methane with micropores in the presence and absence of water. In Section 3.2.1, insights generated from DFT calculations on the adsorption of methane and water on different sites of coal are presented, and in Section 3.2.2, the diffusion of the CH<sub>4</sub>/H<sub>2</sub>O system within micropores of coal is analyzed.

## 2. Materials and Methods

### 2.1. DFT Calculations

We used plane-wave density functional theory (DFT) to predict the adsorption behaviors of methane and water on the coal surfaces at the molecular level. All calculations were performed using the DMol<sup>3</sup> program in the Materials Studio software package. (Version 2017 R2, Dassault Systèmes BIOVIA, San Diego, 5005 Wateridge Vista Drive, CA, USA) [21,22]. The Perdew–Burke–Ernzerhof (PBE) [23] form of the generalized gradient approximation (GGA) was used as the exchange–correlation functional. Grimme’s DFT-D method was adopted to account for the dispersion effect [24]. We also tested other forms of functionals, including revised PBE (RPBE) [25] and Becke–Lee–Yang–Parr (BLYP) [26] forms of GGA functionals, as well as two typical higher-level meta-GGA functionals, namely m11-L [27] and revtpss [28], but found that PBE coupled with DFT-D can closely reproduce the well-established adsorption energy value of methane on the surface of graphene, while keeping the computational cost reasonably low. A detailed comparison between functionals is given in Section 3.1.1. The triple numerical plus polarization (TNP) basis set (version 4.4) was used in all DFT calculations [21]. All other parameters related to the electronic and geometric steps were set to the default values at the fine level provided by the DMol<sup>3</sup> program.

Coal is a chemical complex consists of C, O, H, N, and S. It does not have a fixed molecular structure and can be subdivided into different types, including anthracite coals, bituminous coals, subbituminous coals, and lignite coals, depending on the concentration of the C element [29]. In this study, we focused on bituminous coals and selected three classical molecular models, which are shown in Figure 1a–c, to simulate the coalbed. In this paper, these three models in Figure 1a–c are referred to as Given type 1 model (G1) [30], Given type 2 model (G2) [31], and Fuchs–Sandoff (FS) model [32], respectively, according to their original references. We chose these three models because they contain a wide range of structural elements and functional groups, including but not limited to aromatic planes, alkane chains, hydroxyl groups, carbonyl groups, and pyridine. These models can represent different structures of coal molecules. As shown later in Section 3.1, although our calculations were based on these three bituminous coals molecules, the results are general and can be extended to other types of coals.

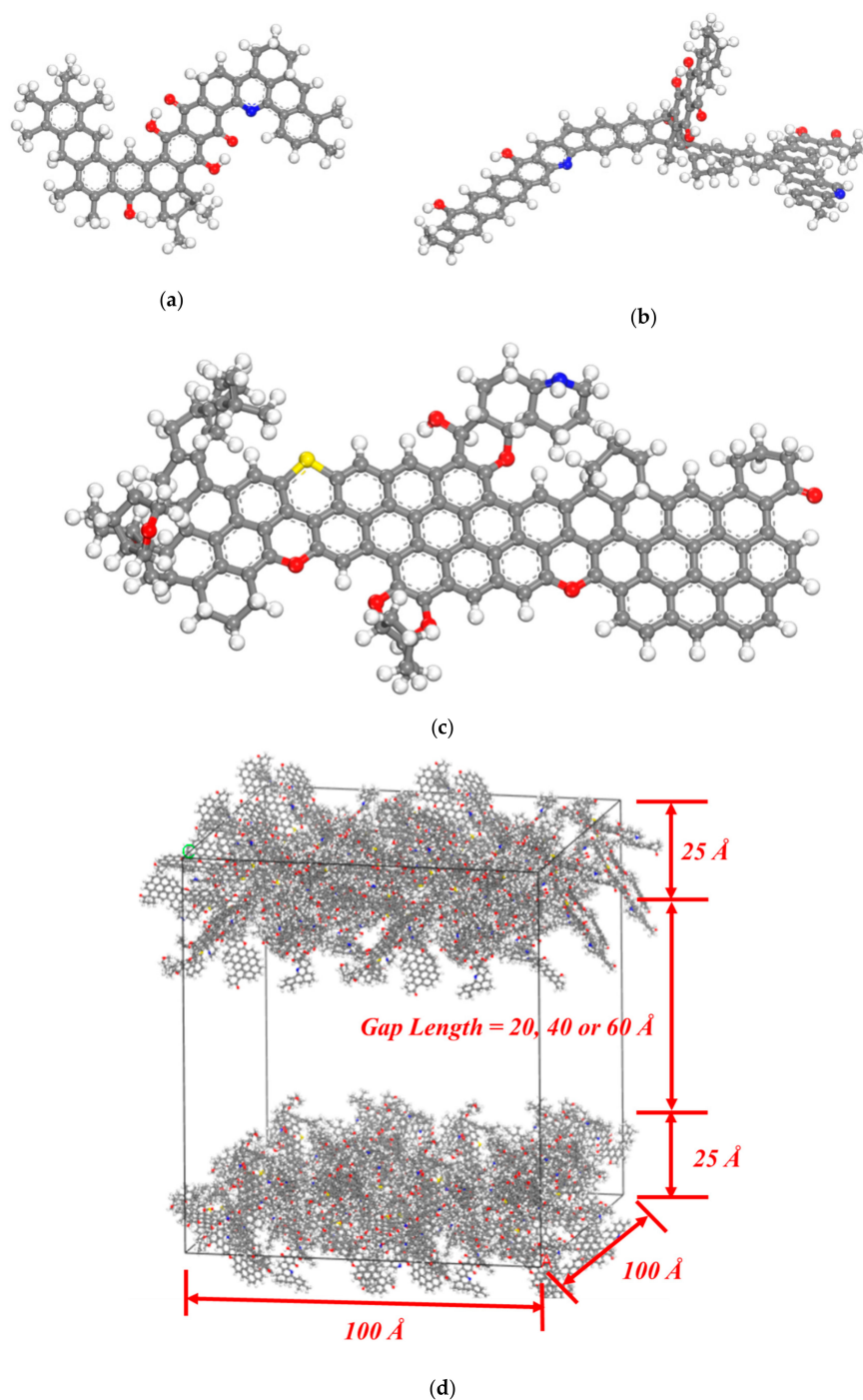


**Figure 1.** Molecular models for coal used in this study. (a) The Given type 1 (G1) model, (b) the Given type 2 (G2) model, and (c) the Fuchs-Sandoff (FS) model were used in the first-principles density-functional theory (DFT) calculations, while the large-cell model in (d) was used in molecular dynamics (MD) studies.

## 2.2. Molecular Simulation

Molecular simulation methods were used to study the desorption and diffusion of  $\text{CH}_4$  in coalbed. The coalbed model used in this study is shown in Figure 1d, which is a large periodic cell with both length and width being 100 Å. This model was obtained from an amorphous cell construction from 80 G1 molecules, 80 FS molecules, and 8 G2 molecules. The cell contains 16,736 C atoms, 13,712 H atoms, 1200 O atoms, 176 N atoms, 80 S atoms, and, therefore, totally 31,904 atoms. The upper and

lower part of the amorphous cell was separated by 20 Å, 60 Å and 100 Å, respectively, to create a gap which represents micropores in the coalbed where CH<sub>4</sub> and H<sub>2</sub>O can be adsorbed.

Methane and water were represented by full atomic models. The COMPASS forcefield was used in this work [33]. Electrostatic interactions were calculated by using forcefield assigned charges. The summation methods for electrostatic and van der Waals interactions were Ewald and atom-based, respectively.

Grand canonical Monte Carlo (GCMC) simulations were used to calculate the adsorption isotherms of CH<sub>4</sub>, H<sub>2</sub>O and the mixture of CH<sub>4</sub> and H<sub>2</sub>O at various pressures in coalbed with different pore sizes. The temperature was fixed at 318.15 K (45 °C) since this is a typical coalbed temperature in coalbed gas extraction processes. For each case, 10<sup>4</sup> configurations at equilibrium were generated and the configuration with the lowest energy was used as the initial input in a MD simulation.

The MD simulations were performed in the constant-temperature, constant-volume (NVT) ensemble with a Nosé–Hoover thermostat to calculate the diffusivities [34]. The cutoff radius of 15.5 Å and time step of 1 fs were used. During simulations, the coalbed model atoms were kept fixed. The diffusion coefficients were calculated by the mean squared displacement (MSD) based on the Einstein relation given by Equation (1).

$$D = \lim_{t \rightarrow \infty} \frac{1}{6tN} \sum_{k=1}^N |r_k(t) - r_k(0)|^2, \quad (1)$$

where  $N$  is the number of CH<sub>4</sub> molecules, and  $r_k(t)$  is the position of the C atom of the  $k$ -th CH<sub>4</sub> molecule at time  $t$ .

### 3. Results and Discussion

#### 3.1. DFT Calculated CH<sub>4</sub> and H<sub>2</sub>O Adsorption on Coal

##### 3.1.1. CH<sub>4</sub> and H<sub>2</sub>O Adsorption on Graphene

Graphene, or a single layer of carbon rings, was often used as a simplified model for coal in previous studies [5,9,35]. In this work, CH<sub>4</sub> and H<sub>2</sub>O adsorptions on graphene were tested in order to validate our computational methods, as well as to provide a baseline for the binding affinity to CH<sub>4</sub> and H<sub>2</sub>O.

The most stable adsorption geometries of CH<sub>4</sub> and H<sub>2</sub>O on graphene predicted by the PBE functional with DFT-D dispersion corrections are shown in Figure 2. Table 1 lists the adsorption energies ( $E_{\text{ads}}$ ) calculated by the PBE+DFT-D and other methods, along with the distances between the graphene plane and the CH<sub>4</sub> or H<sub>2</sub>O molecules.

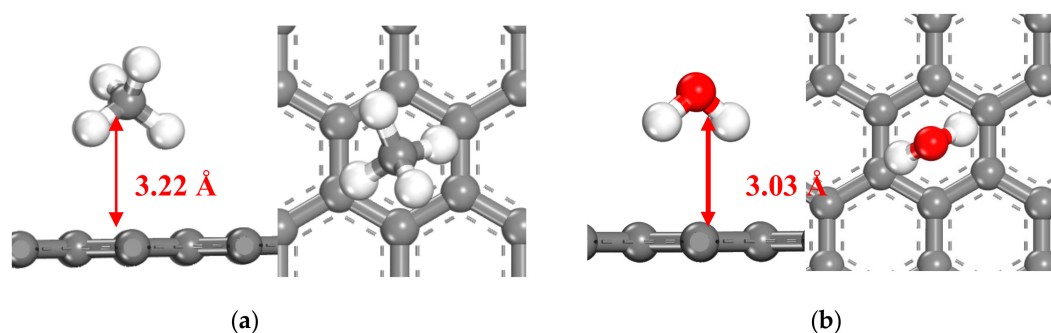


**Figure 2.** Most stable adsorption geometries of (a) CH<sub>4</sub> and (b) H<sub>2</sub>O on graphene.

**Table 1.** Binding energies and distances of CH<sub>4</sub> and H<sub>2</sub>O on the graphene predicted by different DFT functionals and the COMPASS forcefield. For Perdew–Burke–Ernzerhof (PBE) and BLYP functionals, we also tested the effect if no dispersion corrections are considered. Binding energy  $E_{\text{ads}}$  is defined as  $E_{\text{ads}} = E(\text{surface} + \text{adsorbate}) - E(\text{surface}) - E(\text{adsorbate})$ . A more negative  $E_{\text{ads}}$  value means stronger binding. For comparison, values from previous theoretical and experimental studies are also included. RPBE = revised PBE.

Method	CH <sub>4</sub>		H <sub>2</sub> O	
	$E_{\text{ads}}$ (kJ/mol)	Distance (Å)	$E_{\text{ads}}$ (kJ/mol)	Distance (Å)
PBE+DFT-D	−24.90	3.22	−31.63	3.03
PBE (no dispersion)	−8.24	3.58	−7.12	3.19
BLYP+DFT-D	−29.24	3.19	−28.26	3.03
BLYP (no dispersion)	−0.63	4.60	−12.54	3.30
RPBE	−4.62	3.96	−6.68	3.64
m11-L	−29.47	2.87	−29.48	3.10
revtpss	−4.59	3.22	−11.37	3.17
COMPASS forcefield	−5.38	3.47	−20.19	3.36
Literature (DFT)	−31.8 [36]	3.36 [36]	−17.4 [37]	3.25 [37]
Experimental	−13.5 [38]	3.03 [38]	−19.0 [39]	-

The binding energy (−24.90 kJ/mol) and distance (3.22 Å) of CH<sub>4</sub> adsorption on graphene predicted by PBE+DFT-D closely match the experimental values of −13.5 kJ/mol and 3.03 Å [38]. They also resemble the values found in previous theoretical calculations; for example, −31.8 kJ/mol and 3.36 Å, as reported by [36]. A similar study based on a smaller carbon model (C<sub>6</sub>H<sub>8</sub>) predicted the adsorption energy and distance to be −13.3~−13.89 kJ/mol and 3.36~3.39 Å [5].

The results in Table 1 suggest that the dispersion effect is indispensable for the correct prediction of CH<sub>4</sub> and H<sub>2</sub>O adsorption since, without dispersion, the interactions between the carbon layer and the small molecules become rather weak so that the equilibrium distances are larger than the experimental value. The results also suggest that PBE+DFT-D can achieve accuracy equivalent to that produced by m11-L, which is a meta-GGA functional and computational more expensive [27]. Moreover, H<sub>2</sub>O adsorption is slightly stronger (−31.63 kJ/mol) than CH<sub>4</sub> adsorption (−24.90 kJ/mol), with both hydrogen atoms facing towards the graphene layer.

As a comparison, we also tested the accuracy of the COMPASS forcefield. For methane adsorption, the COMPASS forcefield predicted value (−5.38 kJ/mol) is slightly weaker than the experimental result (−13.5 kJ/mol) but is qualitative correct. For H<sub>2</sub>O adsorption, COMPASS forcefield generates an adsorption energy (−17.4 kJ/mol) rather close to the experimental value. The results suggest that the accuracy of the COMPASS forcefield is adequate for the molecular simulation calculations performed in this study.

### 3.1.2. CH<sub>4</sub> and H<sub>2</sub>O Adsorption on Coal Molecules

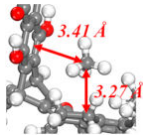
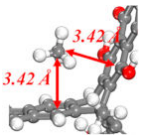
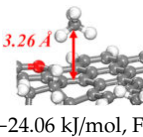
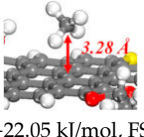
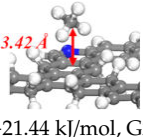
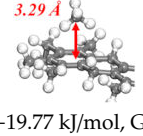
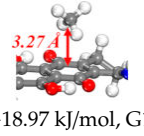
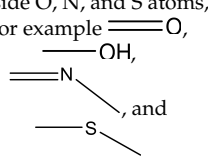
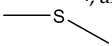
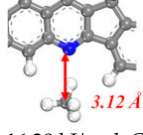
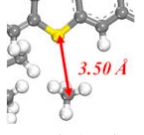
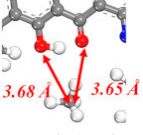
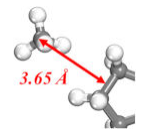
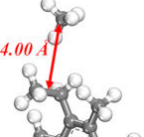
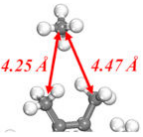
We calculated the adsorption of CH<sub>4</sub> and H<sub>2</sub>O on various sites on the three representative coal molecules as described in Section 2. The results suggest that the binding affinity of CH<sub>4</sub> and H<sub>2</sub>O to coal is primarily determined by the local chemical environment, i.e., the functional groups, on the coal molecules. Chemical compositions and structures of the portions on the coal molecules which are greater than 5 Å away from the CH<sub>4</sub> or H<sub>2</sub>O molecule have little effect on the binding energy. Table 2 enumerates the binding energies of CH<sub>4</sub> versus the functional groups, beside which CH<sub>4</sub> is adsorbed. For each type of adsorption site, several typical adsorption structures are shown, along with their respective adsorption energies. Table 3 gives the same information for H<sub>2</sub>O adsorption.

Several observations can be made based on the results in Tables 2 and 3.

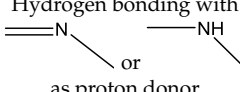
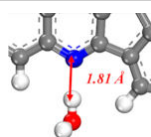
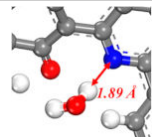
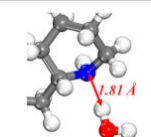
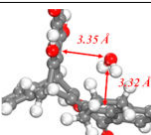
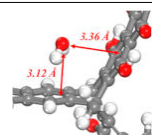
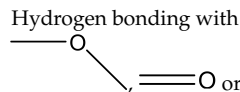
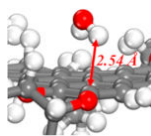
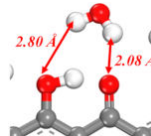
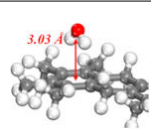
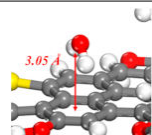
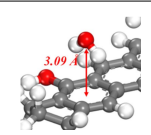
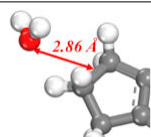
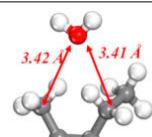
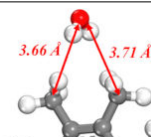
1. The most stable adsorption site for CH<sub>4</sub> is above aromatic planes, especially if a CH<sub>4</sub> molecule interacts with more than one aromatic planes, such as the case in row 1 of Table 2. Polycyclic

- aromatic planes, which resemble the graphene plane, have slightly stronger bind affinity with CH<sub>4</sub>, than monocyclic aromatic planes.
- The most stable adsorption site for H<sub>2</sub>O is N atom sites with H<sub>2</sub>O can form strong hydrogen bonds with N. However, considering that the percentage of the N element in coal is rather low, the amount of H<sub>2</sub>O molecule that can be attracted in coal by N atoms by hydrogen bonding is limited.
  - Water can form hydrogen bonds with O atoms or be adsorbed on aromatic planes, both of which have similar adsorption energies (around -33 kJ/mol). The adsorption of H<sub>2</sub>O on aromatic planes is slightly stronger than CH<sub>4</sub> adsorption, which has E<sub>ads</sub> values around 20 kJ/mol. However, this difference is not large enough to allow the coal surface to have a strong binding preference with H<sub>2</sub>O.
  - The presence of substituents on the aromatic rings, such as hydroxyl, carbonyl, -O-, -N=, and -S-groups, often have little influence (<5 kJ/mol) on the adsorption energies of CH<sub>4</sub> and H<sub>2</sub>O.
  - The least favorable adsorption sites for both CH<sub>4</sub> and H<sub>2</sub>O are alkane groups and chains. It suggests that the molecular surfaces of anthracite coals, which have high carbon concentrations, should have stronger binding affinity with CH<sub>4</sub> and H<sub>2</sub>O than bituminous coals, subbituminous coal, and lignite. This observation is consistent with previous findings that methane binding is stronger on larger aromatic planes [5]. However, this observation does not necessarily suggest that anthracite coals have stronger methane holding capacity, since other morphological factors, including pore sizes and specific surface areas, can also influence the methane sorption behaviors of coals.

**Table 2.** CH<sub>4</sub> adsorption structures and energies on different types of adsorption sites of coal. For each adsorption structure, the adsorption energy (in kJ/mol) and the name of the coal molecule (the codenames G1, G2, and FS refer to Given type 1, Given type 2, and FS, as shown in Figure 1a–c, respectively).

No.	Adsorption Site	Representative Adsorption Structures and Energies		
1	Sandwiched by aromatic planes	 -37.92 kJ/mol, G2	 -27.37 kJ/mol, G2	
2	Above polycyclic aromatic planes such as or	 -24.06 kJ/mol, FS	 -22.05 kJ/mol, FS	 -21.44 kJ/mol, G2
3	Above an aromatic ring with or without substituents	 -19.77 kJ/mol, G1	 -18.97 kJ/mol, G1	 -17.46 kJ/mol, G2
4	Beside O, N, and S atoms, for example  and 	 -16.28 kJ/mol, G1	 -14.36 kJ/mol, FS	 -13.26 kJ/mol, G1
5	Beside alkane groups or chains, such as -CH <sub>3</sub> , -C <sub>2</sub> H <sub>5</sub> , -C <sub>2</sub> H <sub>4</sub> , ...	 -7.96 kJ/mol, G2	 -7.25 kJ/mol, G1	 -5.90 kJ/mol, G1

**Table 3.** H<sub>2</sub>O adsorption structures and energies on different types of adsorption sites of coal.

No.	Adsorption Site	Representative Adsorption Structures and Energies		
1	Hydrogen bonding with  as proton donor	 -54.33 kJ/mol, G2	 -48.48 kJ/mol, G1	 -46.06 kJ/mol, FS
2	Sandwiched by aromatic planes	 -41.30 kJ/mol, G2	 -33.87 kJ/mol, G2	
3	Hydrogen bonding with  OH as proton donor or acceptor	 -33.54 kJ/mol, FS	 -33.49 kJ/mol, G2	 -31.39 kJ/mol, G1
4	Above monocyclic or polycyclic aromatic planes	 -33.49 kJ/mol, G1	 -32.40 kJ/mol, FS	 -29.47 kJ/mol, G2
5	Beside alkane groups or chains such as -CH <sub>3</sub> , -C <sub>2</sub> H <sub>5</sub> , -C <sub>2</sub> H <sub>4</sub> -, ...	 -9.38 kJ/mol, G2	 -9.19 kJ/mol, G1	 -8.04 kJ/mol, G1

The above observations were made based on the assumptions that an isolated CH<sub>4</sub> or H<sub>2</sub>O molecule was adsorbed on the surface. In fact, both CH<sub>4</sub> and H<sub>2</sub>O can be present on the surface at the same time. In the next section, we examine the co-adsorption of CH<sub>4</sub> and H<sub>2</sub>O.

### 3.1.3. Co-Adsorption of CH<sub>4</sub> and H<sub>2</sub>O on Coal Molecules

As demonstrated in Section 3.1.2, both CH<sub>4</sub> and H<sub>2</sub>O prefer aromatic planes over alkane chains. Therefore, CH<sub>4</sub> and H<sub>2</sub>O may be adsorbed competitively on the aromatic planes of coal. To quantitatively investigate their intermolecular interactions, we examined the co-adsorption of CH<sub>4</sub> and H<sub>2</sub>O and calculated the adsorption energy of CH<sub>4</sub> in the presence of a nearby H<sub>2</sub>O and vice versa. The geometries and energies of six co-adsorption structures are shown in Figure 3.

A comparison between Figure 3a,c and row 4 of Table 3 suggest that the presence of a nearby CH<sub>4</sub> has a negligible influence on the adsorption of H<sub>2</sub>O, even if the distance between CH<sub>4</sub> and H<sub>2</sub>O is as small as 3.43 Å. The same conclusion holds for CH<sub>4</sub> adsorption. As shown in Figure 3d,f and row 2 of Table 2, the adsorption energy of CH<sub>4</sub> above aromatic planes is around 22 kJ/mol, regardless of whether a nearby H<sub>2</sub>O molecule is present.

The results in Figure 3 suggest CH<sub>4</sub> and H<sub>2</sub>O have rather weak interactions. They will neither enhance nor weaken the adsorption of each other. The results also imply that H<sub>2</sub>O does not have the ability to dispel CH<sub>4</sub> from the coal surface if CH<sub>4</sub> is already adsorbed on the surface. Water is usually found in CBM wells. In some cases, water coexists with coal in the well, and the CBM well needs to be dewatered before the extraction. In other instances where the CBM wells are fractured, external water is introduced through the fracturing fluid. This conclusion implies that water does not facilitate the desorption of CH<sub>4</sub> from the coalbed. In Section 3.2, the effect of water on the desorption of CH<sub>4</sub> from the coal surface is further investigated from the MD point of view.

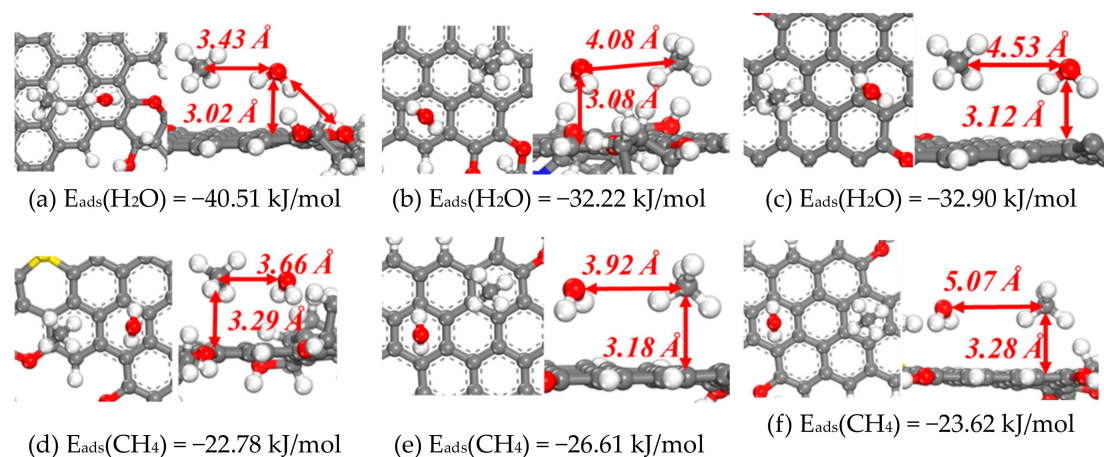


**Figure 3.**  $\text{CH}_4$  and  $\text{H}_2\text{O}$  co-adsorption geometries and energies. Panel (a–c) show different adsorption structures and energies of  $\text{H}_2\text{O}$  with the presence of a  $\text{CH}_4$  molecule. Panel (d–f) show the adsorption structures and energies of  $\text{CH}_4$  with the presence of an  $\text{H}_2\text{O}$  molecule. For each structure, a top view and a side view are given.

### 3.2. MD Simulation of $\text{CH}_4$ Desorption and Diffusion in Coalbed

In Section 3.1, we analyzed the adsorption of  $\text{CH}_4$  and  $\text{H}_2\text{O}$  on the surface of coal molecules using DFT calculations. However, the results in Section 3.1 are from a static point of view. They provide limited information for the dynamic desorption and diffusion process of  $\text{CH}_4$  in a coalbed with the presence of fracturing fluid, which is crucial in coalbed gas extraction processes. In this section, we use MD methods to simulate the desorption and diffusion of  $\text{CH}_4$  with and without the presence of  $\text{H}_2\text{O}$ .

#### 3.2.1. Adsorption Isotherms

The adsorption isotherms of  $\text{CH}_4$  on coal models with varying pore sizes were tested using the GCMC method. Two sets of calculations were performed. In the first set, the adsorption of pure  $\text{CH}_4$  was considered. In the second set, a mixture of  $\text{CH}_4$  and  $\text{H}_2\text{O}$ , in which the fugacity of both  $\text{CH}_4$  and  $\text{H}_2\text{O}$  are equal to the values marked on the x-axis, was loaded into the cell. Isotherms generated by these two sets of calculations are shown in Figure 4a,b, respectively.

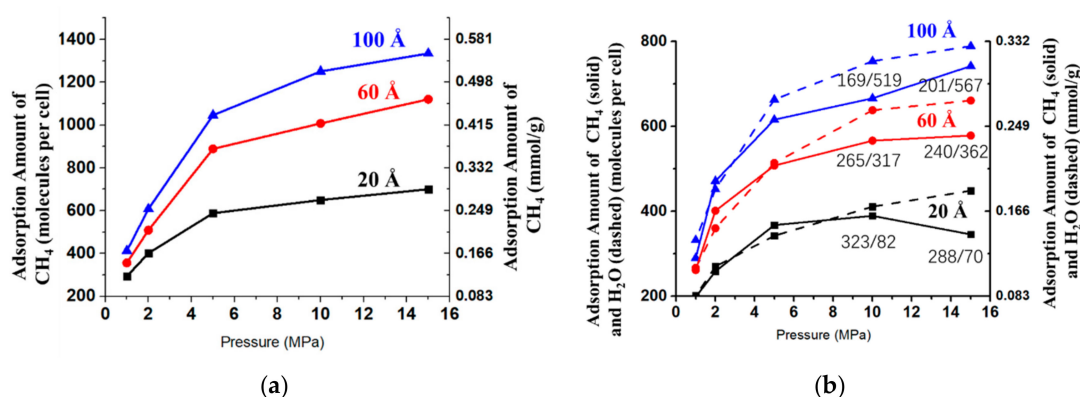


**Figure 4.** Adsorption isotherms of (a)  $\text{CH}_4$  and (b)  $\text{CH}_4$  and  $\text{H}_2\text{O}$  in the coalbed model. Blue, red, and black lines refer to the models with 100 Å, 60 Å, and 20 Å pore sizes, respectively. For convenience, the adsorption amounts are measured in units of both the number of molecules per cell and mmol/g (by assuming that the coal has a specific surface area of 50  $\text{m}^2/\text{g}$ ). In (a),  $\text{CH}_4$  is the only adsorbate. In (b), both  $\text{CH}_4$  (solid lines) and  $\text{H}_2\text{O}$  (dashed lines) with equal fugacity are adsorbed in the cell.

Figure 4a suggests that the adsorption amount increases as the pore size and pressure become larger. However, the adsorption amount of the coalbed structure with 100 Å pore size is much less

than five times of that with the 20 Å pore size. A more careful analysis shows that, under 15 MPa, 300 adsorbed and 1079 free CH<sub>4</sub> molecules are in the 100 Å pore size model, if we consider CH<sub>4</sub> molecules that are within 5 Å of the coal surface to be adsorbed. While in the 60 Å and 20 Å pore size models, the adsorbed/free CH<sub>4</sub> molecules are 392/820 and 498/225, respectively. Therefore, the number of free CH<sub>4</sub> is strictly proportional to the pore size, while at the same time a larger pore size promotes the desorption of CH<sub>4</sub> from the surface when the pressure is kept constant.

When a mixture of CH<sub>4</sub> and H<sub>2</sub>O was considered, the adsorption amounts of CH<sub>4</sub> and H<sub>2</sub>O as functions of pore sizes and pressures are shown in Figure 4b. As represented by the solid curves, the adsorption amount of CH<sub>4</sub> increases as the pressure becomes higher in the models with 100 Å and 60 Å pore sizes, while in the 20 Å model, the adsorption amount of CH<sub>4</sub> slightly decreases as the pressures changes from 10 MPa to 15 MPa. Therefore, in the small pore size case, increasing the pressure of H<sub>2</sub>O contributes to the desorption of CH<sub>4</sub> from the coal surface; however, this strategy does not apply to cases where the pore sizes are large.

### 3.2.2. Diffusivity of CH<sub>4</sub>

MD simulations were performed to investigate the diffusivity of CH<sub>4</sub> both in the presence and absence of water. The diffusion coefficients of CH<sub>4</sub> under different pressures and in models with varying pore sizes are shown in Figure 5.

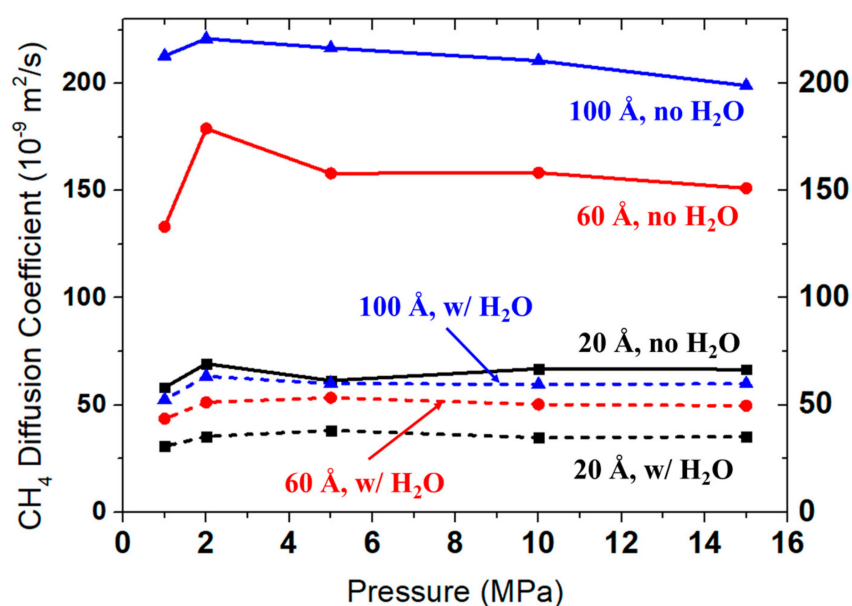


**Figure 5.** Diffusion coefficients of CH<sub>4</sub> in the coalbed models with varying pore sizes. Solid and dashed lines show the cases where CH<sub>4</sub> alone or a mixture of CH<sub>4</sub> and H<sub>2</sub>O is adsorbed in the cell, respectively. Blue, red, and black lines represent the results generated from models with 100 Å, 60 Å, and 20 Å pore sizes, respectively.

The most obvious observation from Figure 5 is that, with H<sub>2</sub>O present, the diffusion of CH<sub>4</sub> is significantly impeded. If mixed with H<sub>2</sub>O, the diffusion coefficients of CH<sub>4</sub> are reduced to only one fourth to one half compared with the cases when only CH<sub>4</sub> is considered. The reason is that H<sub>2</sub>O molecules, which can form a hydrogen-bond network, can partially trap CH<sub>4</sub> molecules to reduce their mobility. This effect, sometimes known as the WBE, can be observed in coalbed extraction processes [38]. Residual fracturing fluid can be present at the entrance of micropores in the coalbed and act like seals to prevent methane from leaving those pores.

The results also suggest that the pressure does not have a strong influence on the diffusivity of CH<sub>4</sub>, while the diffusion coefficient of CH<sub>4</sub> is higher in larger pores. In small pores, such as in the 20 Å

case, the rugged surface and small crevices within the pore may trap CH<sub>4</sub> molecules and hinder the movement of CH<sub>4</sub>.

#### 4. Conclusions

In this study, we used a combined DFT and molecular simulation approach to study the adsorption and diffusion of methane and water in coal. The results show that the most favorable adsorption sites for methane on coal molecules are aromatic planes. Although water can form hydrogen bonds with O or N atoms in coal, its adsorption energies on aromatic planes, which are the main adsorption sites for methane, are only slightly stronger than that of methane. There is also little mutual influence between water and methane on their separate adsorption energies if they are co-adsorption on the coal surface. These observations suggest water does not compete strongly with methane in the adsorption on coal molecular surfaces. Further MD studies indicate that the WBE on methane diffusion since the diffusivity of methane is significantly reduced when water is present. This study can provide insights into the fundamental reasons behind the WBE. Future works will be focused on the design and verification of strategies that can alleviate the WBE, including the screening of proper surfactants and the removal of water by creating pore negative pressures.

**Author Contributions:** Conceptualization, Y.Y. and W.L.; methodology, L.L.; software, W.L., C.C.; validation, L.L., M.L. and X.Z.; formal analysis, C.Y.; investigation, Y.W.; resources, B.F.; data curation, Y.Y.; writing—original draft preparation, L.L.; writing—review and editing, W.L.; visualization, C.Y.; supervision, Y.W.; project administration, Y.Y., W.L.; funding acquisition, Y.Y., L.L. and W.L.

**Funding:** This research was funded by National Science and Technology Major Project, China, grant number 2017ZX05064.

**Acknowledgments:** Computational resources were provided by the National Supercomputing Center in Shenzhen.

**Conflicts of Interest:** The authors declare no conflict of interest.

#### References

1. Moore, T.A. Coalbed Methane: A Review. *Int. J. Coal Geol.* **2012**, *101*, 36–81. [[CrossRef](#)]
2. Mastalerz, M. Chapter 7—Coal Bed Methane: Reserves, Production and Future Outlook. In *Future Energy*, 2nd ed.; Letcher, T.M., Ed.; Elsevier: Boston, MA, USA, 2014; pp. 145–158.
3. Qin, Y.; Moore, T.A.; Shen, J.; Yang, Z.; Shen, Y.; Wang, G. Resources and Geology of Coalbed Methane in China: A Review. *Int. Geol. Rev.* **2018**, *60*, 777–812. [[CrossRef](#)]
4. Su, X.; Wang, Q.; Lin, H.; Song, J.; Guo, H. A Combined Stimulation Technology for Coalbed Methane Wells: Part 1. Theory and Technology. *Fuel* **2018**, *233*, 592–603. [[CrossRef](#)]
5. Qiu, N.-X.; Xue, Y.; Guo, Y.; Sun, W.-J.; Chu, W. Adsorption of Methane on Carbon Models of Coal Surface Studied by the Density Functional Theory Including Dispersion Correction (DFT-D3). *Comput. Theor. Chem.* **2012**, *992*, 37–47. [[CrossRef](#)]
6. Yu, S.; Bo, J.; Fengjuan, L. Competitive Adsorption of CO<sub>2</sub>/N<sub>2</sub>/CH<sub>4</sub> onto Coal Vitrinite Macromolecular: Effect of Electrostatic Interactions and Oxygen Functionalities. *Fuel* **2019**, *235*, 23–38. [[CrossRef](#)]
7. Yutong, F.; Yu, S. CO<sub>2</sub>-Adsorption Promoted CH<sub>4</sub>-Desorption onto Low-Rank Coal Vitrinite by Density Functional Theory Including Dispersion Correction (DFT-D3). *Fuel* **2018**, *219*, 259–269. [[CrossRef](#)]
8. Xu, H.; Chu, W.; Huang, X.; Sun, W.; Jiang, C.; Liu, Z. CO<sub>2</sub> Adsorption-Assisted CH<sub>4</sub> Desorption on Carbon Models of Coal Surface: A DFT Study. *Appl. Surf. Sci.* **2016**, *375*, 196–206. [[CrossRef](#)]
9. Liu, X.-Q.; Xue, Y.; Tian, Z.-Y.; Mo, J.-J.; Qiu, N.-X.; Chu, W.; Xie, H.-P. Adsorption of CH<sub>4</sub> on Nitrogen- and Boron-Containing Carbon Models of Coal Predicted by Density-Functional Theory. *Appl. Surf. Sci.* **2013**, *285*, 190–197. [[CrossRef](#)]
10. Pini, R.; Ottiger, S.; Storti, G.; Mazzotti, M. Prediction of Competitive Adsorption on Coal by a Lattice DFT model. *Adsorption* **2010**, *16*, 37–46. [[CrossRef](#)]
11. Yu, S.; Yan-ming, Z.; Wu, L. Macromolecule Simulation and CH<sub>4</sub> Adsorption Mechanism of Coal Vitrinite. *Appl. Surf. Sci.* **2017**, *396*, 291–302. [[CrossRef](#)]
12. Hu, H.; Du, L.; Xing, Y.; Li, X. Detailed Study on Self- and Multicomponent Diffusion of CO<sub>2</sub>-CH<sub>4</sub> Gas Mixture in Coal by Molecular Simulation. *Fuel* **2017**, *187*, 220–228. [[CrossRef](#)]

13. Zhou, W.; Wang, H.; Zhang, Z.; Chen, H.; Liu, X. Molecular Simulation of CO<sub>2</sub>/CH<sub>4</sub>/H<sub>2</sub>O Competitive Adsorption and Diffusion in Brown Coal. *RSC Adv.* **2019**, *9*, 3004–3011. [[CrossRef](#)]
14. Dang, Y.; Zhao, L.; Lu, X.; Xu, J.; Sang, P.; Guo, S.; Zhu, H.; Guo, W. Molecular Simulation of CO<sub>2</sub>/CH<sub>4</sub> Adsorption in Brown Coal: Effect of Oxygen-, Nitrogen-, and Sulfur-Containing Functional Groups. *Appl. Surf. Sci.* **2017**, *423*, 33–42. [[CrossRef](#)]
15. Xiang, J.; Zeng, F.; Liang, H.; Li, B.; Song, X. Molecular Simulation of the CH<sub>4</sub>/CO<sub>2</sub>/H<sub>2</sub>O Adsorption onto the Molecular Structure of Coal. *Sci. China Earth Sci.* **2014**, *57*, 1749–1759. [[CrossRef](#)]
16. Zhang, J.; Liu, K.; Clennell, M.B.; Dewhurst, D.N.; Pervukhina, M. Molecular Simulation of CO<sub>2</sub>–CH<sub>4</sub> Competitive Adsorption and Induced Coal Swelling. *Fuel* **2015**, *160*, 309–317. [[CrossRef](#)]
17. Huang, W.; Lei, M.; Qiu, Z.; Leong, Y.-K.; Zhong, H.; Zhang, S. Damage Mechanism and Protection Measures of a Coalbed Methane Reservoir in the Zhengzhuang Block. *J. Nat. Gas Sci. Eng.* **2015**, *26*, 683–694. [[CrossRef](#)]
18. Su, X.; Wang, Q.; Song, J.; Chen, P.; Yao, S.; Hong, J.; Zhou, F. Experimental Study of Water Blocking Damage on Coal. *J. Pet. Sci. Eng.* **2017**, *156*, 654–661. [[CrossRef](#)]
19. Ni, G.; Cheng, W.; Lin, B.; Zhai, C. Experimental Study on Removing Water Blocking Effect (WBE) from Two Aspects of the Pore Negative Pressure and Surfactants. *J. Nat. Gas Sci. Eng.* **2016**, *31*, 596–602. [[CrossRef](#)]
20. Ni, G.; Li, Z.; Xie, H. The Mechanism and Relief Method of the Coal Seam Water Blocking Effect (WBE) Based on the Surfactants. *Powder Technol.* **2018**, *323*, 60–68. [[CrossRef](#)]
21. Delley, B. Ground-State Enthalpies: Evaluation of Electronic Structure Approaches with Emphasis on the Density Functional Method. *J. Phys. Chem. A* **2006**, *110*, 13632–13639. [[CrossRef](#)]
22. Delley, B. Time Dependent Density Functional Theory with Dmol3. *J. Phys. Condens. Matter* **2010**, *22*, 384208. [[CrossRef](#)] [[PubMed](#)]
23. Perdew, J.P.; Burke, K.; Ernzerhof, M. Generalized Gradient Approximation Made Simple. *Phys. Rev. Lett.* **1996**, *77*, 3865–3868. [[CrossRef](#)] [[PubMed](#)]
24. Grimme, S.; Antony, J.; Ehrlich, S.; Krieg, H. A Consistent and Accurate Ab Initio Parametrization of Density Functional Dispersion Correction (DFT-D) for the 94 Elements H–Pu. *J. Chem. Phys.* **2010**, *132*, 154104. [[CrossRef](#)] [[PubMed](#)]
25. Hammer, B.; Hansen, L.B.; Nørskov, J.K. Improved Adsorption Energetics within Density-Functional Theory Using Revised Perdew–Burke–Ernzerhof Functionals. *Phys. Rev. B* **1999**, *59*, 7413–7421. [[CrossRef](#)]
26. Becke, A.D. A Multicenter Numerical Integration Scheme for Polyatomic Molecules. *J. Chem. Phys.* **1988**, *88*, 2547–2553. [[CrossRef](#)]
27. Peverati, R.; Truhlar, D.G. M11-L: A Local Density Functional That Provides Improved Accuracy for Electronic Structure Calculations in Chemistry and Physics. *J. Phys. Chem. Lett.* **2012**, *3*, 117–124. [[CrossRef](#)]
28. Tao, J.; Perdew, J.P.; Staroverov, V.N.; Scuseria, G.E. Climbing the Density Functional Ladder: Nonempirical Meta-Generalized Gradient Approximation Designed for Molecules and Solids. *Phys. Rev. Lett.* **2003**, *91*, 146401. [[CrossRef](#)] [[PubMed](#)]
29. Jonathan, P.; Mathews, A.L.C. The Molecular Representations of Coal—A Review. *Fuel* **2012**, *96*, 1–14.
30. Given, P. Advances in organic geochemistry the Chemical Study of Coal Macerals. In *The Chemical Study of Coal Macerals, Proceedings of the International Meeting in Milan, Milan, Italy, 8–11 September 2019*; Hobson, G.D., Speers, G.C., Eds.; Macmillan: New York, NY, USA, 1962; pp. 39–48.
31. Given, P. The Distribution of Hydrogen in Coals. *Fuel* **1960**, *39*, 147–153.
32. Fuchs, W.; Sandhoff, A.G. Theory of Coal Pyrolysis. *Ind. Eng. Chem.* **1942**, *34*, 567–571. [[CrossRef](#)]
33. Sun, H. Compass: An Ab Initio Force-Field Optimized for Condensed-Phase Applications overview with Details on Alkane and Benzene Compounds. *J. Phys. Chem. B* **1998**, *102*, 7338–7364. [[CrossRef](#)]
34. Hoover, W. Canonical Dynamics: Equilibrium Phase-Space Distributions. *Phys. Rev. A* **1985**, *31*, 1695–1697. [[CrossRef](#)] [[PubMed](#)]
35. Nie, B.; Wang, L.; Li, X.; Wang, C.; Li, L. Simulation of the Interaction of Methane, Carbon Dioxide and Coal. *Int. J. Min. Sci. Technol.* **2013**, *23*, 919–923. [[CrossRef](#)]
36. Vidali, G.; Ihm, G.; Kim, H.-Y.; Cole, M.W. Potentials of Physical Adsorption. *Surf. Sci. Rep.* **1991**, *12*, 135–181. [[CrossRef](#)]
37. Li, K.; Li, H.; Yan, N.; Wang, T.; Zhao, Z. Adsorption and Dissociation of CH<sub>4</sub> on Graphene: A Density Functional Theory Study. *Appl. Surf. Sci.* **2018**, *459*, 693–699. [[CrossRef](#)]

38. Alfarge, D.K.; Wei, M.; Bai, B. Numerical simulation study of factors affecting relative permeability modification for water-shutoff treatments. *Fuel* **2017**, *207*, 226–239. [[CrossRef](#)]
39. Jenness, G.R.; Karalti, O.; Jordan, K.D. Benchmark Calculations of Water–Acene Interaction Energies: Extrapolation to the Water–Graphene Limit and Assessment of Dispersion–Corrected Dft Methods. *Phys. Chem. Chem. Phys.* **2010**, *12*, 6375–6381. [[CrossRef](#)] [[PubMed](#)]



© 2019 by the authors. Licensee MDPI, Basel, Switzerland. This article is an open access article distributed under the terms and conditions of the Creative Commons Attribution (CC BY) license (<http://creativecommons.org/licenses/by/4.0/>).